PCCP

XANES analysis of phosphate glasses melted with Tb_4O_7 and SnO: Evaluating the impact of valence states on structural, thermal, and luminescent properties

Journal:	*Physical Chemistry Chemical Physics*
Manuscript ID	CP-ART-10-2023-004784.R1
Article Type:	Paper
Date Submitted by the Author:	16-Nov-2023
Complete List of Authors:	Jiménez, José; Georgia Southern University, Chemistry and Biochemistry Hayes, Dugan; University of Rhode Island College of Arts and Sciences, Department of Chemistry Antolini, Cali; University of Rhode Island College of Arts and Sciences, Department of Chemistry Reinhart, Benjamin; Argonne National Laboratory Advanced Photon Source

XANES analysis of phosphate glasses melted with Tb_4O_7 and SnO: Evaluating the impact of valence states on structural, thermal, and luminescent properties

José A. Jiménez [a,*], Dugan Hayes[b], Cali Antolini[b], Benjamin J. Reinhart[c]

[a] *Department of Biochemistry, Chemistry, and Physics, Georgia Southern University, Statesboro, GA 30460, USA*

[b] *Department of Chemistry, University of Rhode Island, Kingston, Rhode Island 02881, USA*

[c] *X-ray Science Division, Argonne National Laboratory, Argonne, Illinois 60439, USA*

*Corresponding author. E-mail: jjimenez@georgiasourthern.edu

ORCID:

José A. Jiménez: **0000-0001-9256-3836**

Dugan Hayes: **0000-0003-4171-5179**

Cali Antolini: **0000-0002-5081-6724**

Benjamin J. Reinhart: **0000-0001-5654-8823**

Abstract Barium phosphate glasses were prepared with 0.5 mol% Tb_4O_7 added alongside SnO up to 5 mol% with the purpose of evaluating the resulting terbium and tin oxidation states and their impact on glass structural, thermal, and luminescent properties. Following material synthesis by melt-quenching, the composition-structure-property investigation was pursued encompassing measurements by X-ray diffraction (XRD), X-ray absorption near-edge spectroscopy (XANES), Raman spectroscopy, differential scanning calorimetry (DSC), dilatometry, and photoluminescence (PL) spectroscopy. While XRD confirmed the amorphous nature of the glasses, results from XANES indicated that terbium occurs as terbium(III) with a predisposition for tin to exist as tin(IV) which decreased at high SnO content. The structural as well as the thermal properties appeared to be mostly impacted by the presence of tin(IV). Specifically, glass depolymerization was indicated to be induced by Sn^{4+} ions, and their concentration was observed to correlate with glass transition and softening temperatures. On the other hand, the tin(II) remnants were observed to exert an impact on the luminescent properties shifting light emission from the green towards the blue-green (cyan). It is indicated that Tb_4O_7 reacting to produce Tb_2O_3 supports the oxidation of tin(II) to tin(IV) which in turn dominates the physical properties. However, this was somewhat circumvented at the highest SnO content wherein tin(IV) appeared to be lower.

Keywords: glasses; luminescence; rare earths; structural properties; thermal properties

1. Introduction

The development of luminescent Tb^{3+}-containing materials has been an active area of research given the various potential applications, which span from optical devices (e.g., lighting and scintillators),[1-9] to sensing and chemical analysis.[10-13] The utility for light-emitting devices (LEDs) has been particularly stimulating in the pursuit of efficient energy use and reducing environmental impact.[13,14] Such applications take advantage of the characteristic green emission of terbium(III) which makes it a valuable component to obtain white light emission together with blue- and red-emitting species in inorganic materials.[4,15-19] In this context, divalent tin (e.g., added as SnO) has been considered an interesting ns^2-type center with blue-emitting character.[4,5,19] Further, as first reported by Blinov et al.[20] and supported by the work of Wang and Gan[4], Sn^{2+} ions can act as sensitizers for Tb^{3+} ions in glasses, thus enhancing their green-emitting character. Inorganic glasses are appealing as hosts for optical applications given the relative ease of preparation (e.g., by melting), versatility for compositional variation, and adequate optical, thermal, and mechanical properties attainable through the choice of constituents. As highlighted by the works of Wang and Gan[4], Lv et al.[5] and Masai et al.[19] also encompassing Sn^{2+} and Tb^{3+} codoping, phosphate glasses are especially attractive due to the low-melting character, low production costs, and high solubility for the rare-earth ions.

A common way to obtain Tb^{3+} ions is by addition of the readily-available terbium(III,IV) oxide (Tb_4O_7)[2,8,10] which decomposes and releases O_2 as

$$2Tb_4O_7 \rightarrow 4Tb_2O_3 + O_2\uparrow \quad (1)$$

The effect that the oxidizing character of Tb_4O_7 has on the different constituents of a glass material during material preparation is thus of interest from fundamental and applied

perspectives.[8] Still, the impact of melting phosphate glasses with Tb_4O_7 and SnO jointly on the resulting terbium and tin valence states, and consequent glass physicochemical properties have not been reported to the best of the authors' knowledge.

In this framework, the present work encompassing a composition-structure-property investigation was carried out to study the effects of Tb_4O_7 and SnO as codopants in phosphate glasses. Specifically, the resulting terbium and tin oxidation sates were analyzed, and their impact on structural, thermal, and luminescent properties was assessed. A binary barium phosphate glass matrix previously studied with other metals and rare-earths was used as host.[21-23] The glasses were synthesized by melt-quenching with fixed Tb_4O_7 amounts at 0.5 mol% and increasing SnO content added up to 5 mol% (both relative to network former P_2O_5). The glasses were then characterized by X-ray diffraction (XRD) to confirm amorphous nature, and by X-ray absorption near-edge structure (XANES) spectroscopy at the Sn K-edge and Tb L_3-edge for tin and terbium speciation analysis. Subsequently, the evaluation of structural and thermal properties was pursued by Raman spectroscopy, differential scanning calorimetry (DSC), and dilatometry, seeking to understand the impact of tin oxidation. The photoluminescence (PL) properties were ultimately assessed in connection with Sn^{2+} and Tb^{3+} occurrence and their contribution to light emission evaluated.

2. Experimental

2.1. Glass synthesis

Phosphate glasses containing terbium and tin were prepared by the melting technique based on the $50BaO{:}50P_2O_5$ (mol%) glass matrix using high purity compounds P_2O_5 (≥ 98%), $BaCO_3$ (99.8%), Tb_4O_7 (99.9%), and SnO (≥ 99.9%). The doping was made in an additive manner in mol% in relation to network former P_2O_5: the amount of Tb_4O_7 was kept fixed at 0.5 mol%,

while SnO was added incrementally as 1, 3 and 5 mol%. A Tb-doped glass was also made with merely 0.5 mol% Tb_4O_7. The labels used for the different glasses alongside their respective nominal compositions are summarized in Table 1. The raw materials (~25 g batches) were weighed, mixed, and melted in porcelain crucibles at 1150 °C for 15 min under ambient atmosphere conditions. The glasses were annealed at 420 °C for 3 hours to remove mechanical/thermal stress. The glasses were cut and polished to about 1 mm thick slabs for spectroscopic measurements.

Table 1. Glass codes and nominal compositions with additive concentrations (mol%) of Tb_4O_7 and SnO used for the glasses synthesized.

Glass	P_2O_5 (mol%)	BaO (mol%)	Tb_4O_7 (mol%)	SnO (mol%)
Tb	50	50	0.5	—
1SnTb	50	50	0.5	1.0
3SnTb	50	50	0.5	3.0
5SnTb	50	50	0.5	5.0

2.2. Measurements

2.2.1. XRD

XRD was done to confirm non-crystalline nature with a PANalytical Empyrean X-ray diffractometer operating at room temperature (RT) with Cu-Kα radiation (λ = 1.5406 Å). Glass samples were crushed to powder by mortar and pestle for this analysis. The acceleration voltage and current used were 45 kV and current 40 mA, respectively.

2.2.2. XANES

Sn K-edge and Tb L_3-edge XANES spectra of the polished glass slabs were measured under ambient conditions at beamline 12-BM-B of the Advanced Photon Source at Argonne National

Laboratory. The incident X-ray energy was scanned using a Si(311) monochromator with samples mounted 45° relative to the beam, and spectra were acquired *via* fluorescence detection using a 12-element Ge detector. The same sample position was used for all scans of a given sample, and no signs of beam-induced damage (e.g., changes in the XANES spectra) were observed throughout the measurements. All spectra were calibrated, then averaged, and finally normalized in Athena, a part of the Demeter 0.9.25 software package.[24] Tb L_3-edge spectra were calibrated relative to a Tb_4O_7 powder reference spectrum using 7518.8 and 7526.8 keV as the energies of the two white line peaks.[25,26]

Because only small deviations in the Sn K-edge energy were expected between samples, it is crucial to account for any mechanical irreproducibility in the initial position of the monochromator between scans. However, attenuation of the beam by the intact glass samples was too severe to permit simultaneous measurement of an Sn metal reference foil placed after the sample as a reference for the energy axis of each individual scan. Instead, a $Z + 1$ (i.e., Sb) metal reference foil was mounted *before* the sample position. Absolute calibration of the energy axis was attained by measuring transmission spectra of the Sb foil and an Sn foil simultaneously but individually using three ionization chambers (i.e., an ionization chamber on either side of each reference foil). The maximum of the first derivative of the Sn spectrum was then set to 29200.1 eV, and all subsequently measured spectra were then calibrated by aligning the peak of the Sb spectrum to that of the calibrated absolute reference spectrum. XANES spectra were acquired with an energy spacing of 0.4 eV in a 45-eV range about both the Sn and Sb K-edges with broadly spaced points between the edges to facilitate normalization.

Reference spectra of SnO and SnO_2 powders were also collected by fluorescence detection, and these spectra were used as the two standards for linear combination analysis of the glass

samples. This method, which we have previously applied to quantify Sn(II/IV) speciation tin halide perovskite thin films,[27] was further validated by analyzing the spectra of SnO and SnO_2 powder mixtures of known composition.

2.2.3. Raman spectroscopy

Raman spectra were recorded at RT using polished glass slabs with a Thermo Scientific DXR Raman microscope operating at 532 nm and a power of 10 mW. A 10× MPlan objective was employed for data collection with the acquisition time for each spectrum set at 100 s. Baseline subtraction was done using OriginPro, after which the spectra were normalized for comparison.

2.2.4. Thermal analysis

Calorimetric analysis was carried out for the various glasses (30-50 mg samples) in a SDT650 calorimeter (TA Instruments) in alumina pans using a heating rate of 10 °C/min and N_2 gas atmosphere with a flow rate of 100 mL/min. The thermal parameters of glass transition temperature (T_g), onset of crystallization (T_x), and peak crystallization temperature (T_c) were then determined (TRIOS instrument's software; midpoint-inflection approach for T_g).

Dilatometry measurements were carried out on glasses which were quenched in cylindrical shapes and cut to a length of about 2.54 cm. The evaluation was done under ambient atmosphere in an Orton dilatometer (Model 1410B) operating at a heating rate of 3 °C/min. The determination of the various parameters of dilatometric or softening temperature (T_s), the T_g, and linear coefficient of thermal expansion (CTE) was then carried out through the instrument's software.

2.2.5. PL spectroscopy

PL spectroscopy was carried out on the polished glass slabs at RT with a Horiba Fluorolog-QM spectrofluorometer equipped with continuous and pulsed (~2 μs) Xe lamps. The spectra were obtained under static conditions using a step size of 1 nm, whereas emission decay curves were recorded using the Xe flash lamp.

3. Results and discussion

3.1. XRD

X-ray diffraction patterns obtained for the Tb and 1-5SnTb glasses (Table 1) are shown in Fig. 1. The diffractograms analogously exhibit the broad diffuse scattering at lower angles resulting from long-range structural disorder. Besides, no distinct crystallization peaks were detected for any of the samples analyzed. Even though XANES data considered below indicated that SnO oxidation occurred in the 1-5SnTb glasses, SnO_2 crystallites, which would display diffraction peaks for 2θ around 27°, 34° and 52°,[28] were not detected. The data thus supports the overall amorphous nature of the glasses synthesized as well as the incorporation of Sn^{4+} ions produced into the glassy structures (*vide infra*).

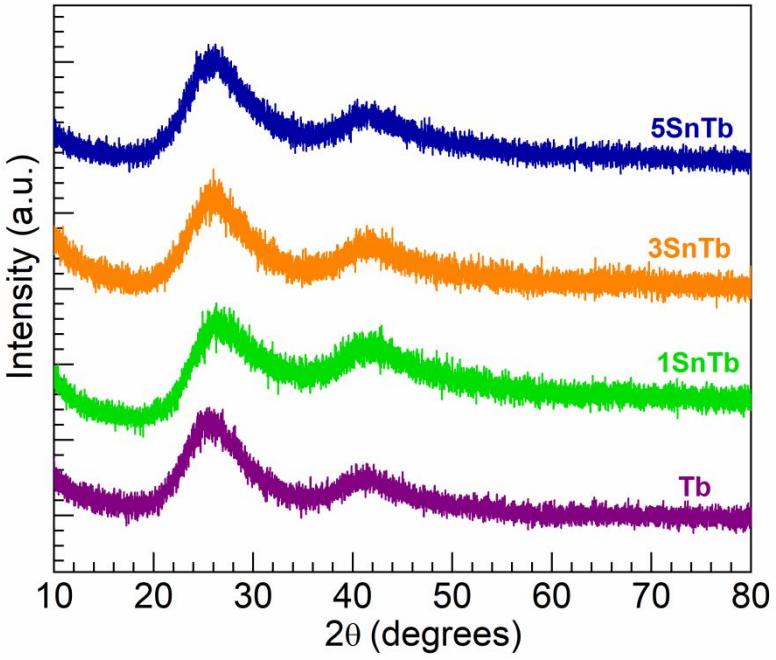

Fig. 1. XRD patterns recorded in the $10° \leq 2\theta \leq 80°$ range for the Tb and 1-5SnTb glasses.

3.2. XANES

As a primary aspect of this work, the elucidation of the oxidation states of both tin and terbium in the codoped glasses is now considered based on X-ray absorption spectroscopy analyses. Figure 2 shows the normalized Sn K-edge XANES spectra obtained for the 1-5SnTb glasses together with the spectra of SnO_2 and SnO as reference materials. The different peak positions detected for the different samples are also labeled in Fig. 2 to aid in the comparisons. It can be noticed that the spectrum of the 1SnTb glass with maximum around 29209.2 eV is in good agreement with the spectrum obtained for the SnO_2 reference, which exhibits a peak at 29209.6 eV. This clearly indicates a prevalence of tin in the 1SnTb glass as Sn^{4+}. However, the 3SnTb and 5SnTb glasses displaying peaks at 29208.8 and 29208.0 eV, respectively, show a propensity towards the SnO reference which has a maximum at about 29206.0 eV. The 3SnTb and 5SnTb glasses do not present an ideal match with either reference, but their spectra instead

lie in between. The behavior is indicative of the occurrence of Sn^{2+} in these glasses together with Sn^{4+}.[27,29] Seeking a quantitative assessment of tin valence states, the Sn K-edge XANES spectra of the 1-5SnTb glasses were fit to linear combinations (LCs) of the SnO_2 and SnO reference spectra as shown in Fig. 3 (a)-(c). The fits, which are also presented in the different panels in Fig. 3, yielded relative amounts of Sn^{4+} in the 1SnTb, 3SnTb and 5SnTb glasses estimated as >99%, 56% and 28%, respectively. Hence, based on the nominal contents of SnO added (mol%) to the glasses as 1%, 3% and 5%, it can be appraised that the concentrations (additive mol%) of Sn^{4+} ions were >0.99%, 1.68% and 1.40%, corresponding to Sn^{2+} then at <0.01%, 1.32% and 3.60%, for the 1SnTb, 3SnTb and 5SnTb glasses, respectively. As will be considered (*vide infra*), the Sn^{4+} contents were observed to correlate with results from the structural and thermal characterizations performed on the glasses.

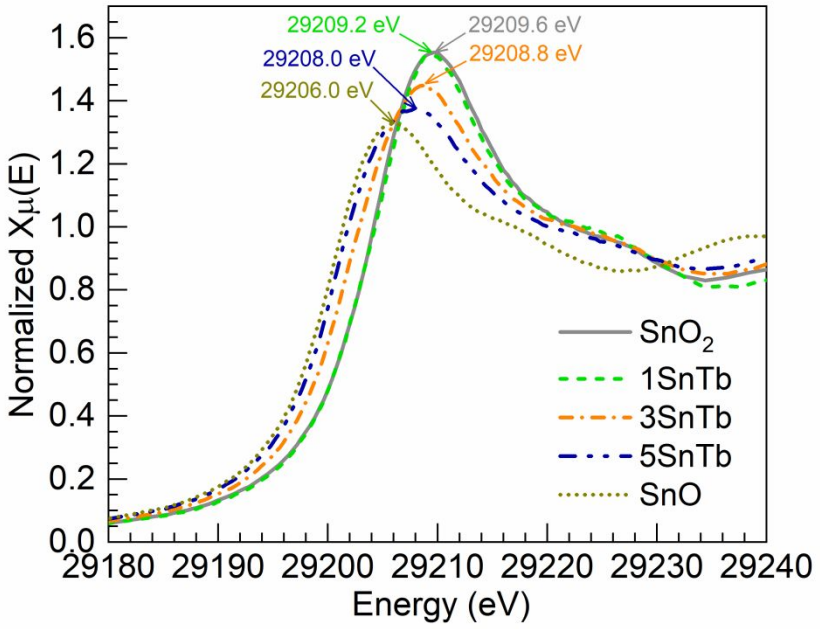

Fig. 2. Normalized Sn K-edge XANES spectra for the 1-5SnTb glasses alongside SnO_2 and SnO as reference materials; the peak positions detected for the reference materials and the different glasses are indicated by the arrows (also color coded).

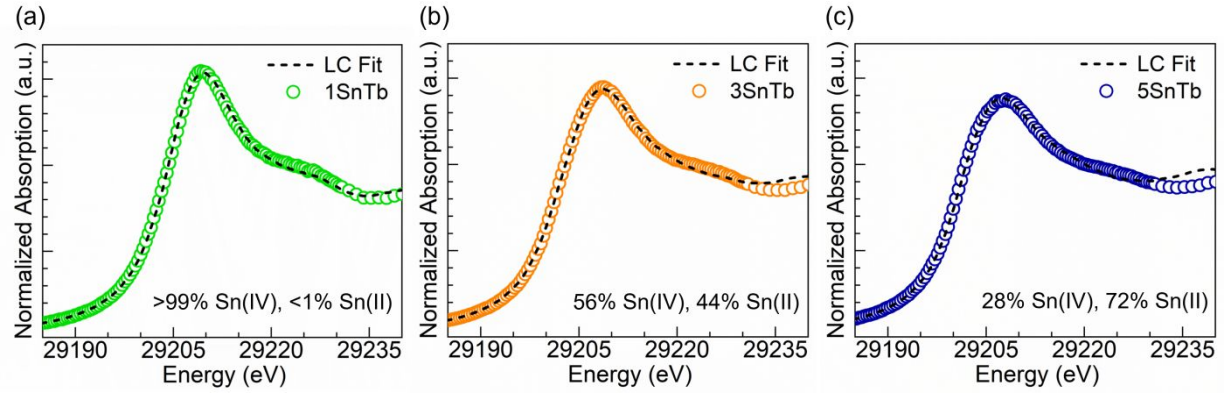

Fig. 3. The Sn K-edge XANES spectra of the 1-5SnTb glasses (open symbols) overlaid with linear combination (LC) fits (dashed traces) used for tin speciation analysis (estimated relative quantities indicated).

The Sn K-edge XANES data obtained indicate that significant oxidation of Sn^{2+} occurred in the glasses during the material preparation phase, however with decreased propensity as the SnO contents increased. Even though the synthesis was carried out under ambient atmosphere, the source of terbium being Tb_4O_7 can be anticipated to exert an oxidizing effect [e.g., Eq. (1)]. To verify the terbium oxidation state in the 1-5SnTb glasses, Tb L_3-edge XANES spectra were obtained, which are shown in Fig. 4 alongside Tb_4O_7 as reference material. The latter standard shows the Tb^{3+} and Tb^{4+} states in the spectrum as well-resolved peaks around 7518.8 and 7526.8 eV, respectively.[30] The 1-5SnTb glasses on the other hand are lacking the Tb^{4+} peak and exhibit a single peak harmonizing with the occurrence of terbium as Tb^{3+} ions.[31] This was noticed even at the lowest tin content in the 1SnTb glass exhibiting a peak in Fig. 4 around 7518.3 eV. The 3SnTb and 5SnTb glasses were then in good resemblance with each other and with the 1SnTb glass. The data thus confirms a $Tb^{4+} \rightarrow Tb^{3+}$ reduction process in the melts. Apart from the

possible Tb_4O_7 decomposition represented by Eq. (1), a redox reaction with SnO in which Tb^{4+} serves as the oxidizing agent could be also contemplated:

$$Tb_4O_7 + SnO \rightarrow 2Tb_2O_3 + SnO_2 \quad (2)$$

However, we cannot conclusively determine the degree to which Tb^{4+} *vs.* O_2 serves to oxidize Sn^{2+} to Sn^{4+} with the current data. As ultimately considered in this work (*vide infra*), the optical properties appear dominated by the green-emitting Tb^{3+} ions alongside Sn^{2+} residuals which contribute with blue luminescence.

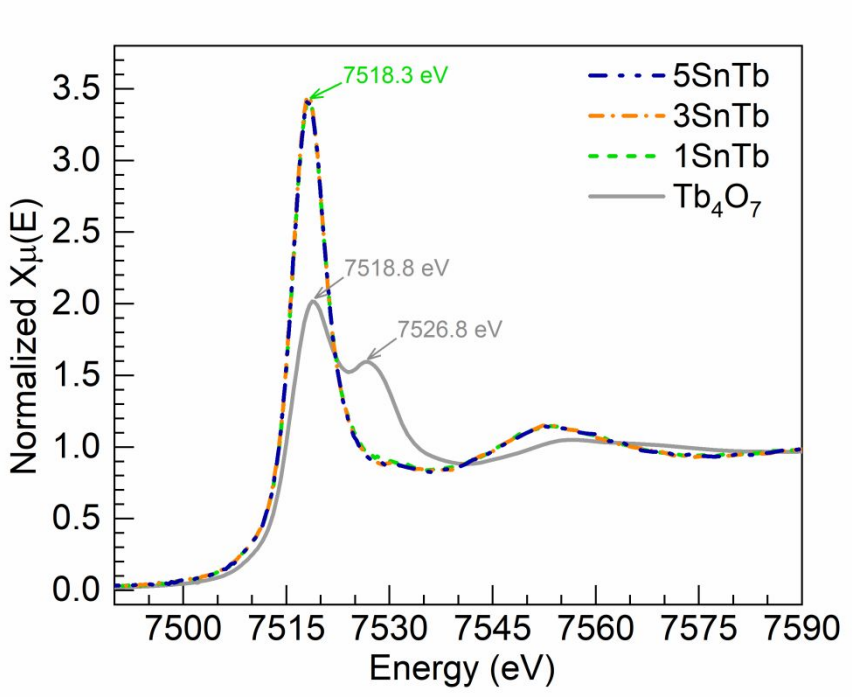

Fig. 4. Tb L_3-edge XANES spectra for the 1-5SnTb glasses alongside Tb_4O_7 as reference material; the peak positions detected for the reference material and 1SnTb glass are indicated by the arrows (also color coded).

3.3. Raman spectroscopy

Raman spectra obtained for the Tb and 1-5SnTb glasses to examine structural properties are shown in Fig. 5. Following baseline subtraction, the spectra were normalized in the 600-1400 cm^{-1} range with respect to the strongest band as presented in Fig. 5 (a). The assignment for the various features is achieved in agreement with the literature as reported for similar phosphate-based glasses.[22,23,32,33] Taken as reference, the Tb glass exhibits towards the low energy region a band around 685 cm^{-1} credited to the in-chain symmetric stretching vibrations in P−O−P bridges, ν_s(POP), in Q^2 tetrahedral units (PO_4 tetrahedra with 2 bridging oxygens, BOs). The small feature observed around 1006 cm^{-1} is attributed to the symmetric stretch, $\nu_s(PO_3^{2-})$, in non-bridging oxygens (NBOs) pertaining to Q^1 units (PO_4 tetrahedra with 1 BO). Then the Tb glass shows the most intense band around 1160 cm^{-1} in connection with the out-of-chain symmetric stretching in PO_2^- groups, $\nu_s(PO_2^-)$, that take place in NBOs belonging to the Q^2 units. Lastly, the asymmetric stretching vibrations in such units, $\nu_{as}(PO_2^-)$, appears as the small feature around 1250 cm^{-1}.

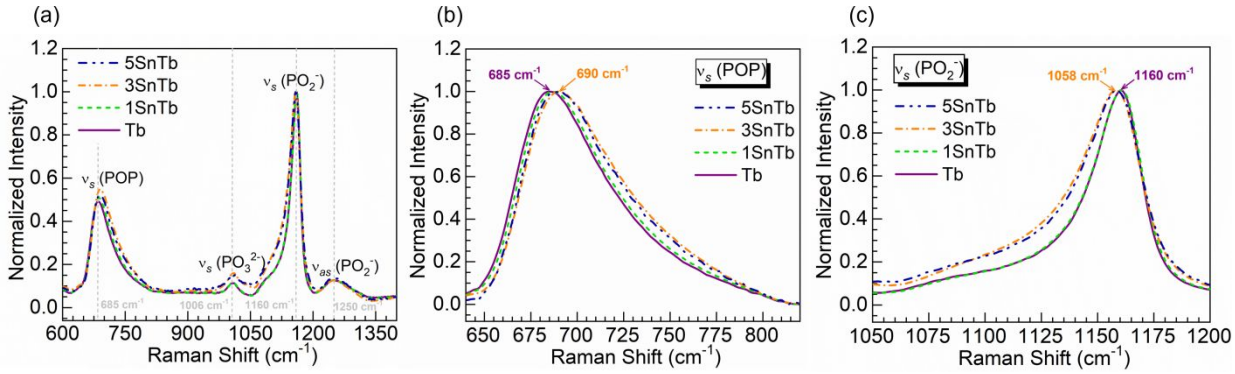

Fig. 5. Raman spectra of the Tb and 1-5SnTb glasses. The spectra are normalized in different spectral ranges: (a) 600-1400 cm^{-1} covering main spectroscopic features (vertical dashed lines mark wavenumbers displayed); (b) 640-820 cm^{-1} range covering the bridging oxygen band, ν_s(POP); and (c) 1050-1200 cm^{-1} range covering the non-bridging oxygen band, $\nu_s(PO_2^-)$. The

peak positions for Tb and 3SnTb glasses are indicated by the arrows (also color coded) in panels (b) and (c).

While the 1SnTb glass spectrum in Fig. 5 (a) appears similar to the Tb glass, the $\nu_s(PO_3^{2-})$ band exhibits an increase in intensity for the 3SnTb and 5SnTb glasses. As this band is a manifestation of NBOs in Q^1 terminal units, its upsurge suggests a depolymerization effect is induced at high tin contents. Some broadening is also noticed concerning the $\nu_s(PO_2^-)$ band (NBO-related), and to some degree the ν_s(POP) band (BO-related). To evaluate these effects more closely, the ν_s(POP) and $\nu_s(PO_2^-)$ bands are presented normalized in Fig. 5 (b) and (c), respectively. The ν_s(POP) band linked to BOs in the Q^2 units is observed to ultimately blue-shift to 690 cm^{-1} for the 3SnTb glass exhibiting broader extension toward the high frequency region. This type of shift accompanied by band broadening has been associated with depolymerization effects in phosphate glasses.[32] Namely, shorter PO_4 tetrahedra chains yield higher frequency components of the ν_s(POP) band, where an asymmetry toward higher frequencies points to asymmetric distributions of chain lengths toward shorter chains.[32] As seen in Fig. 5 (c), a minor red-shift to 1058 cm^{-1} was detected in the 3SnTb glass for the $\nu_s(PO_2^-)$ band dealing with NBOs. However, this band exhibited substantial broadening also pointing to increased heterogeneity of the amorphous PO_2 environment.[32] It is suggested that the overall tin content is not the main reason for the changes, but rather the concentration of a particular oxidation state. In this connection, the different roles of Sn^{2+} and Sn^{4+} on glass structure should be considered.[34-36] Bekaert et al.[34] investigated glasses of xSnO:$(100 - x)$$NaPO_3$ compositions with $x \leq 40$ by nuclear magnetic resonance (NMR) and Mössbauer spectroscopy, and reported that Sn^{2+} exhibited network forming character, while a network modifier role was implied for Sn^{4+} ions.

The network former role of Sn^{2+} was also endorsed by ^{31}P NMR spectroscopy in the work from Jiménez and Zhao[35] in barium phosphate glass with 10 mol% SnO added. Further, the network former and modifier roles of Sn^{2+} and Sn^{4+}, respectively, were supported by ^{31}P NMR and X-ray photoelectron spectroscopy (O 1s and Sn 3d) in tin and rare-earth containing phosphate glasses by Jiménez et al.[36] Accordingly, in the present work the impact of Sn^{4+} ions having a network modifier role are most likely contributing to depolymerization in the phosphate glass, rather than Sn^{2+} which could be inserted in the phosphate network forming P–O–Sn linkages between PO_4 tetrahedra.[36]

To appraise the influence of Sn^{4+} on various spectral effects, in Fig. 6 (a)-(c), the integrated areas of the NBO-$\nu_s(PO_2^-)$ and BO-ν_s(POP) bands, their positions, and their full width at half maximum (FWHM) values are plotted as function of the Sn^{4+} concentration estimated for the glasses from the XANES analysis (*vide supra*). The integrated intensities plotted in Fig. 6 (a), which are based on the bands as presented in Fig. 5 (a), show an increasing trend with overall Sn^{4+} concentration. The 3SnTb glass with $[Sn^{4+}]$ = 1.68% stands out with the highest values next to the 5SnTb glass having $[Sn^{4+}]$ = 1.40%. Additional trends are observed in Fig. 6 (b) and (c) for the positions and FWHM values *vs.* Sn^{4+} contents, respectively, for the two bands deduced from the spectra in Fig. 5 (b) and (c). Most significantly, the parameters of Raman shift and FWHM for the BO-related ν_s(POP) band in Fig. 6 (b) and (c) are seen to increase as function of $[Sn^{4+}]$, concurring with the growth of integrated intensities in Fig. 6 (a). The 3SnTb glass with the highest Sn^{4+} content stands out with the furthermost values just after the 5SnTb glass. Overall, the trends exhibited harmonize with a broader distribution of phosphate chain lengths and higher heterogeneity of the PO_2 environment as expected for an increased depolymerization effect driven by network modifiers.[32,37] The results therefore appear to reflect the modifier role

of Sn^{4+} ions discussed in the literature.[34-36] Conversely, no correlating behavior stands for the various parameters from Raman spectra *vs.* Sn^{2+} concentration increasing in the glasses ([Sn^{2+}] estimated at <0.01%, 1.32% and 3.60% for the 1SnTb, 3SnTb and 5SnTb glasses, correspondingly). Thus, the Raman characterization supports that the structural modifications were driven by the oxidation of SnO possibly in accord with Eq. (2). As will be considered next, a structure-property relationship also appears supported by the results from calorimetric analysis.

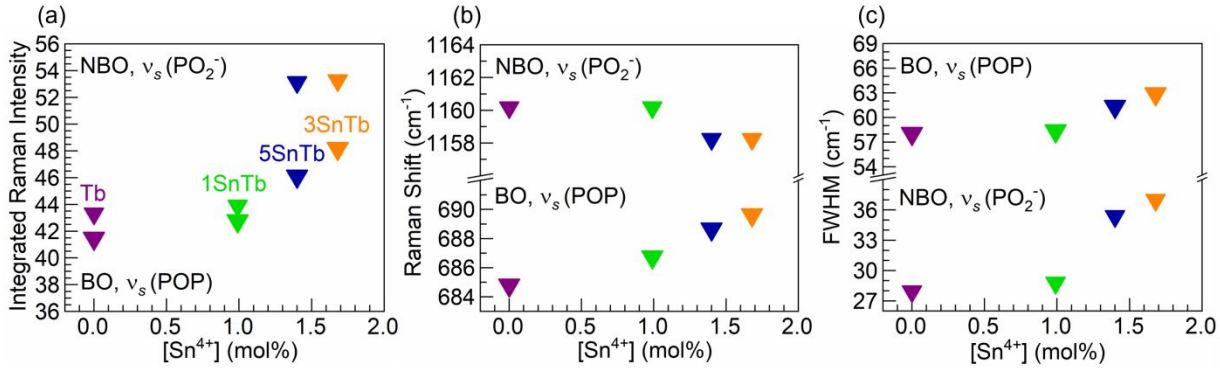

Fig. 6. Parameters from Raman spectra (Fig. 5) plotted as a function of the total Sn^{4+} contents in the glasses estimated based on XANES speciation analysis: (a) integrated intensities of the bridging oxygen (BO) band (bottom triangles) and non-bridging oxygen (NBO) band (top triangles); (b) positions of the BO band (bottom triangles) and NBO band (top triangles); and (c) full width at half maximum (FWHM) of the BO band (top triangles) and NBO band (bottom triangles). The colors of the triangle symbols in all panels follow the sample labels in panel (a): Tb-purple, 1SnTb-green, 3SnTb-orange, and 5SnTb-blue.

3.4. Thermal analysis

Shown in Fig. 7 are the DSC profiles obtained for the Tb and 1-5SnTb glasses within the 300-800 °C range. From these, the peak crystallization temperatures, T_c, the onset of

crystallization, T_x, and glass transition temperatures, T_g, were determined. The corresponding values estimated are marked and indicated in Fig. 7 (color-coded with the different sample traces) and summarized in Table 2. Also presented in Table 2 is the additional parameter $\Delta T = T_x - T_g$ indicating glass stability.[38,39] The Tb glass taken as reference exhibits a single crystallization peak around 706 °C with T_x at 654 °C, and within the glass transition region a T_g value of 505 °C was estimated. The implied stability factor is thus ΔT = 149 °C, which is somewhat lower than that reported for a similar 0.5 mol% Tm_2O_3-doped barium phosphate glass with ΔT of 169 °C, given the T_g, T_x and T_c of 499, 668 and 699 °C, respectively.[22] The slightly lower glass stability in the Tb glass prepared herein may be due to the use of overall marginally higher rare-earth content when using 0.5 mol% Tb_4O_7. The 1SnTb glass then shows in Fig. 7 two crystallization peaks with T_c values shifted to higher temperature relative to the Tb glass, namely at 710 and 766 °C. The T_g of the 1SnTb glass also increased to 512 °C, and ultimately a stability factor of ΔT = 158 °C is obtained (Table 2) which is slightly higher than the Tb glass. It is worth mentioning that for the 1SnTb glass it was found by XANES that most of the tin was oxidized to Sn^{4+}. Thus, the thermal behavior can be credited essentially to tin(IV). The 3SnTb glass then displays a single crystallization event which is somewhat suppressed and has the T_x and T_c at 706 and 744 °C, respectively. The T_g value of 526 °C in 3SnTb is also significantly higher than for 1SnTb, leading to improved glass stability factor ΔT = 180 °C. The quantity of [Sn^{4+}] = 1.68% for the 3SnTb glass thus seems to be greatly impacting the thermal behavior. The high T_g indicates a leading effect of Sn–O bonds strengthening the glass despite the depolymerization effect supported by the Raman spectra (*vide supra*). This is likely due to the high field strength of Sn^{4+} ions acting as network modifiers.[39] Lastly, the 5SnTb glass shows in Fig. 7 a single crystallization peak with T_x and T_c at 698 and 738 °C, respectively, whereas the T_g is estimated at

515 °C. The three parameters are indeed lower than the obtained for the 3SnTb, yet a similar ΔT of 183 °C results (Table 2). Therefore, the total tin content does not seem to be the main cause affecting the thermal behavior. He et al.[39] studied non-alkali aluminoborosilicate glasses containing SnO_2 and reported on their thermal behavior wherein the values of T_g, T_x, T_c, and ΔT first decreased and then increased with tin contents. This complex behavior was indicated by the authors to be related to the mixed valence states of tin ions in the glasses.[39] In binary SnO-P_2O_5 glasses, it has been reported for instance by Cha et al.[40] and Lim et al.[41] that an increase in SnO content tends to slightly increase the T_g. However, the effects become more complicated in ternary phosphate glasses such as the SnO-ZnO-P_2O_5 system studied by Segawa et al.[42] wherein the increase in tin content produced a decrease in T_g values. Here, we consider the oxidative environment and that $[Sn^{4+}]$ = 1.40% for the 5SnTb glass which is lower than the 3SnTb glass with $[Sn^{4+}]$ = 1.68%, which would explain the dissimilar performance. The influence of tin(IV) becomes patent by the T_g *vs.* $[Sn^{4+}]$ plot presented in the inset of Fig. 7. An upward trend is seen with increasing Sn^{4+} concentration in the glasses wherein the 5SnTb glass is positioned between 1SnTb and 3SnTb. It is remarkably consistent with the Raman data plotted in Fig. 6 (a)-(c) following the argument of the tin(IV) content driving the structural modifications. Seeking to complement the thermal characterization, results from dilatometry measurements are considered next.

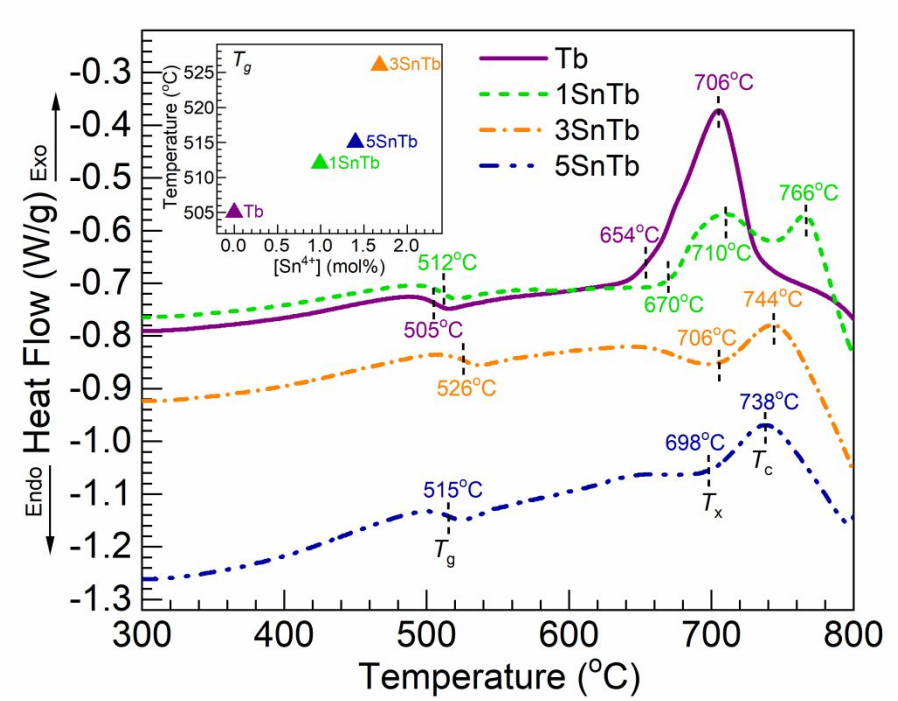

Fig. 7. DSC profiles obtained for the Tb and 1-5SnTb glasses displaying the glass transition (T_g) onset of crystallization (T_x), and crystallization temperatures (T_c) (estimated values indicated and color-coded with the different traces – also presented in Table 2). The inset is a plot of the T_g values deduced as function of the total Sn^{4+} contents estimated by the XANES analysis (labels of corresponding glasses are placed beside symbols).

Table 2. Glass transition temperature (T_g), onset of crystallization (T_x), peak crystallization temperature (T_c), and thermal stability parameter ($\Delta T = T_x - T_g$) estimated for the different glasses by DSC (Fig. 7).

Glass	T_g (°C)	T_x (°C)	T_c (°C)	$\Delta T = T_x - T_g$ (°C)
Tb	505	654	706	149
1SnTb	512	670	710, 766	158
3SnTb	526	706	744	180
5SnTb	515	698	738	183

Figure 8 shows the dilatometric profiles obtained for the glasses under consideration. As exemplified with the Tb glass as reference, the thermal expansion evolution, $dL/L_o(\%)$ *vs. T* (°C), is used to deduce the parameters of T_s, T_g and CTE.[37,43] While the softening temperature, T_s, is readily identified as the peak temperature reached during the expansion, the glass transition regime is more subtle. The T_g is then estimated from the intersection between the line encompassing the initial linear expansion region and a second line covering the linear region representing the increased expansion rate up to T_s. The section wherein the expansion is linear with temperature is then used to determine the CTE. The linear CTE values were estimated for the different glasses in the temperature range starting at 50 °C up to about 25 °C below the T_g[37] (i.e., within 50-466 °C, 50-466 °C, 50-481 °C and 50-477 °C for the Tb, 1SnTb, 3SnTb and 5SnTb glasses, respectively). The values obtained for the T_s, T_g and CTE parameters are summarized in Table 3. Although the estimated T_g values for the Tb and 1SnTb glasses were the same, in general the T_s and T_g values exhibit a trend to increase up to the 3SnTb glass, and then decrease for the 5SnTb glass. Such a turning point agrees with the DSC data discussed above (Fig. 7) supporting a major impact from tin(IV). Consequently, the T_s and T_g values were similarly plotted as functions of the total Sn^{4+} contents estimated from XANES, as shown in the inset of Fig. 8. It is again perceived that an upward trend follows with Sn^{4+} concentration (rather than total tin content), as the 3SnTb glass displayed the highest T_s and T_g values. In harmony with this, Krohn et al.[43] performed dilatometric analysis of tin-doped soda-lime silica glasses and reported a more pronounced effect of SnO_2 than SnO for increasing T_s and T_g. Further, the authors observed that for glasses doped with fixed tin oxide at 2 mol%, the dilatometric and glass transition temperatures decreased with increasing fraction of Sn^{2+}.[43] On the other hand, as seen in

Table 3 the CTE value was herein the lowest for the Tb glass at 13.7 $\times 10^{-6}$ $^{\circ}C^{-1}$, but highest for the 1SnTb glass at 14.7 $\times 10^{-6}$ $^{\circ}C^{-1}$. It then decreased for the 3SnTb and 5SnTb glasses with estimated values of 14.4 $\times 10^{-6}$ $^{\circ}C^{-1}$ and 14.1 $\times 10^{-6}$ $^{\circ}C^{-1}$, respectively. These results indicate that the most compact structure was attained in the Tb glass while the presence of tin mostly as Sn^{4+} in the 1SnTb glass results in decreased rigidity. Thereafter, the 3SnTb and 5SnTb glasses appear to have a tighter structure than 1SnTb. Krohn et al.[43] reported for the tin-doped soda-lime silica glasses that the CTE tends to decrease in a similar manner with SnO *vs*. SnO_2, as the authors obtained similar slopes for the decreasing trends of the CTE values with tin contents. Hence, in the present work it seems that the content of Sn^{2+} increasing in the 3SnTb and 5SnTb glasses to about 1.32% and 3.60%, respectively, exerts an effect on lowering the CTE values relative to the 1SnTb glass. The presence of Sn^{2+} in the 1-5SnTb glasses is further evaluated through the luminescent properties as considered below.

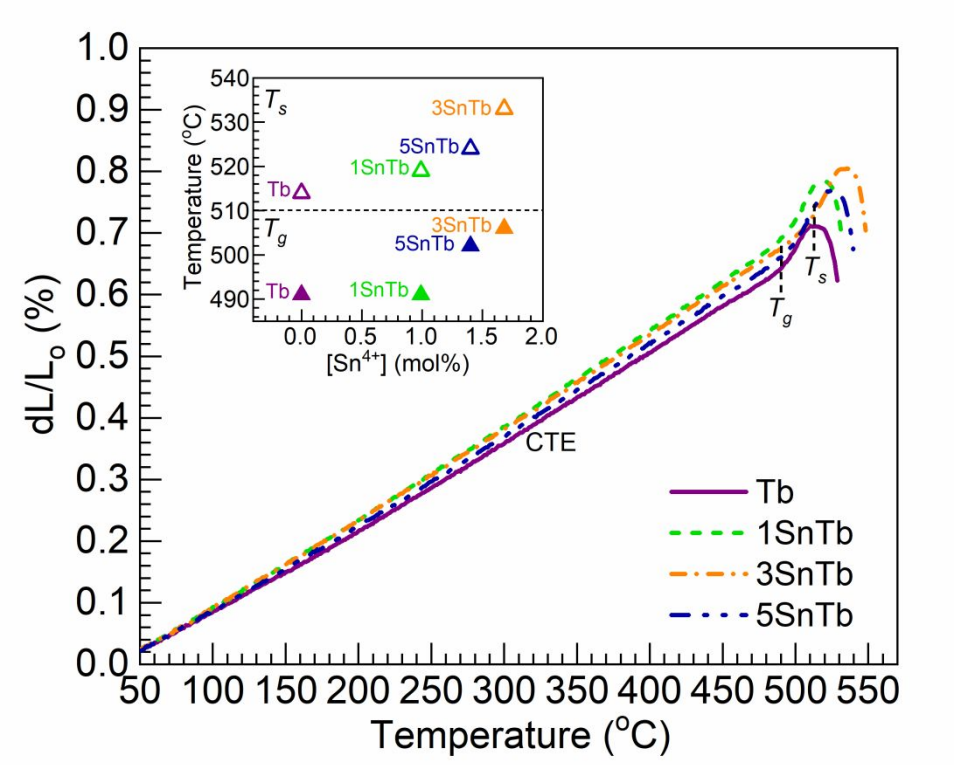

Fig. 8. Dilatometric profiles obtained for the Tb and 1-5SnTb glasses. The regions related to the softening temperature (T_s), the glass transition temperature (T_g), and the linear coefficient of thermal expansion (CTE) are identified with the trace for the Tb glass (the values estimated are presented in Table 3). The inset plots the T_s and T_g values as function of the total Sn^{4+} contents estimated from the XANES analysis; the dashed horizontal line is intended to separate the two parameters – open triangles T_s, solid triangles T_g (labels of corresponding glasses are placed beside symbols).

Table 3. Thermal parameters of softening temperature (T_s), glass transition temperature (T_g), and linear coefficient of thermal expansion (CTE) estimated for the Tb and 1-5TbSn glasses by dilatometry (Fig. 8).

Glass	T_s (°C)	T_g (°C)	CTE ($\times 10^{-6}$ °C^{-1})
Tb	514	491	13.7
1SnTb	519	491	14.7
3SnTb	533	506	14.4
5SnTb	524	502	14.1

3.5. PL spectroscopy

Emission spectra obtained for the Tb and 1-5SnTb glasses are shown in Fig. 9 (a) as recorded under excitation at 265 nm. This wavelength was chosen aiming for the excitation of divalent tin centers in the 1-5SnTb glasses. In fact, while the Tb glass exhibits characteristic emission lines due to $^5D_3 \rightarrow {}^7F_6$, $^7F_5$, $^7F_4$ and $^5D_4 \rightarrow {}^7F_6$, $^7F_5$, $^7F_4$, $^7F_3$ transitions in Tb^{3+} ions as seen in other glass systems,[2-4] the spectra of the tin-containing glasses also present a broad

emission band beneath the Tb^{3+} transitions. The occurrence of this broad PL band can be ascribed to triplet-to-singlet transitions ($T_1 \rightarrow S_0$) in Sn^{2+}.[4,5,21,29,35] It is the weakest for the 1SnTb glass, yet still noticeable despite the detected Sn^{2+} by XANES in such glass being less than 0.01% of the total 1% SnO content added. The 3SnTb and 5SnTb glasses then show augmented broad PL bands. This harmonizes with the increasing Sn^{2+} concentrations estimated by XANES of about 1.32% and 3.60% in the 3SnTb and 5SnTb glasses, respectively. However, the broad emission band does not appear to grow in proportion to the increase in Sn^{2+} content in these glasses. For instance, Sn^{2+} PL intensity at 425 nm which excludes Tb^{3+} emission increases by about 2.3× for the 3SnTb glass relative to the 1SnTb glass with remarkably low Sn^{2+} content, and ~1.2× for 5SnTb relative to 3SnTb. This is likely due to the energy transfer from Sn^{2+} as sensitizer to Tb^{3+} as activator ions.[4,19,20] In the lack of energy transfer processes including self-quenching, the PL from the emitting specie should follow the increase in concentration.[37] On the other hand, in the case where the sensitizer transfers the energy non-radiatively to the activator, its PL is uniformly suppressed contrasting with a radiative transfer.[44] Wang and Gan[4] reported in this context that with the addition of Tb^{3+} the Sn^{2+} emission intensity in lithium-zinc phosphate glasses decreased systematically due to the $Sn^{2+} \rightarrow Tb^{3+}$ energy transfer. Masai et al.[19] also studied the Sn^{2+} PL intensity in SnO-ZnO-P_2O_5 glasses and reported the decrease with the increase in Tb^{3+} content (also for other rare-earths) following the sensitization effect supported by decreased Sn^{2+} lifetimes.

In the inset of Fig. 9 (a), excitation spectra obtained for the glasses are shown, which were recorded by monitoring the emission from $^5D_4 \rightarrow {}^7F_5$ transitions in Tb^{3+} ions at 542 nm, as this wavelength shows the highest ratio of Tb^{3+} emission *vs.* the Sn^{2+} background. The Tb glass displays characteristic Tb^{3+} excitation peaks[2,3] with an additional broader band around 260 nm

likely due to charge transfer transitions.[45] Further, the 1-5SnTb glasses show an amplified excitation band that grows with increasing tin content in the 1-5SnTb glasses, although not in proportion to the increase in Sn^{2+} content analogous to the broad emission band in Fig. 9 (a) as discussed above. The development of such a UV excitation band harmonizes with singlet-to-singlet excitation ($S_0 \rightarrow S_1$) in Sn^{2+}.[4,5,35] It further supports the $Sn^{2+} \rightarrow Tb^{3+}$ energy transfer process first reported by Blinov et al.[20] and confirmed by the work of Wang and Gan.[4] This enhances the green-emitting character of the glasses, while tin(II) also directly contributes with blue emission, which has been considered of interest for developing LEDs.[4] It can be pointed out that the Tb^{3+} emission in Fig. 9 (a), most notably the $^5D_4 \rightarrow {}^7F_5$ transition around 542 nm, increases for the 1-5SnTb glasses relative to the Tb reference. For such emission, the intensity increase is about 1.6× for the 1SnTb glass compared to the Tb glass, ~1.7× for 3SnTb compared to 1SnTb, and ~1.3× for 5SnTb relative to 3SnTb. Since the broad Sn^{2+} emission band contributes to the intensity therein, its exclusion was attempted by baseline subtraction. The Tb^{3+} emission increments at 542 nm were then estimated at ~1.3× for the 1SnTb glass compared to the Tb glass, ~1.7× for 3SnTb compared to 1SnTb, and ~1.3× for 5SnTb relative to 3SnTb. Thus, Tb^{3+} emission increased with Sn^{2+} content apart from the broad PL from Sn^{2+}. Given that the amount of Tb^{3+} is fixed in all the glasses, this shows that the enhancement of Tb^{3+} emission occurred due to sensitization effect from Sn^{2+}. Nonetheless, the Tb^{3+} intensification factors do not follow the Sn^{2+} increments estimated by XANES (*vide supra*) illustrating that the energy transfer efficiencies can still improve. This suggests there is room for optimization, for instance concerning the donor-acceptor distances[44] which could be adjusted by varying Tb^{3+} concentration. Another possibility is that the presence of Sn^{4+} ions is detrimental to the emission

efficiency of Tb^{3+} ions. Even though this aspect would require further research, it appears supported by the lifetime assessment below.

To further characterize the collective light-emitting behavior of the glasses studied, the PL spectra in Fig. 9 (a) were analyzed *via* the Commission Internationale de l'Eclairage (CIE) 1931 chromaticity diagram. The diagram with the chromaticity results is shown in Fig. 9 (b); the inset shows sample photographs taken in dark for the Tb and 1SnTb glasses under excitation at 265 nm for appreciation of the difference in light emission conferred by tin. The (x, y) chromaticity coordinates determined for the Tb, 1SnTb, 3SnTb and 5SnTb glasses were (0.273, 0.480), (0.233, 0.313), (0.231, 0.303), and (0.230, 0.303), respectively. Thus, while the Tb glass emits in the green, the 1-5SnTb glasses produce combined blue-green (cyan) emission, which is qualitatively characterized with a slight shift towards the blue in the 5SnTb glass with highest Sn^{2+} content.

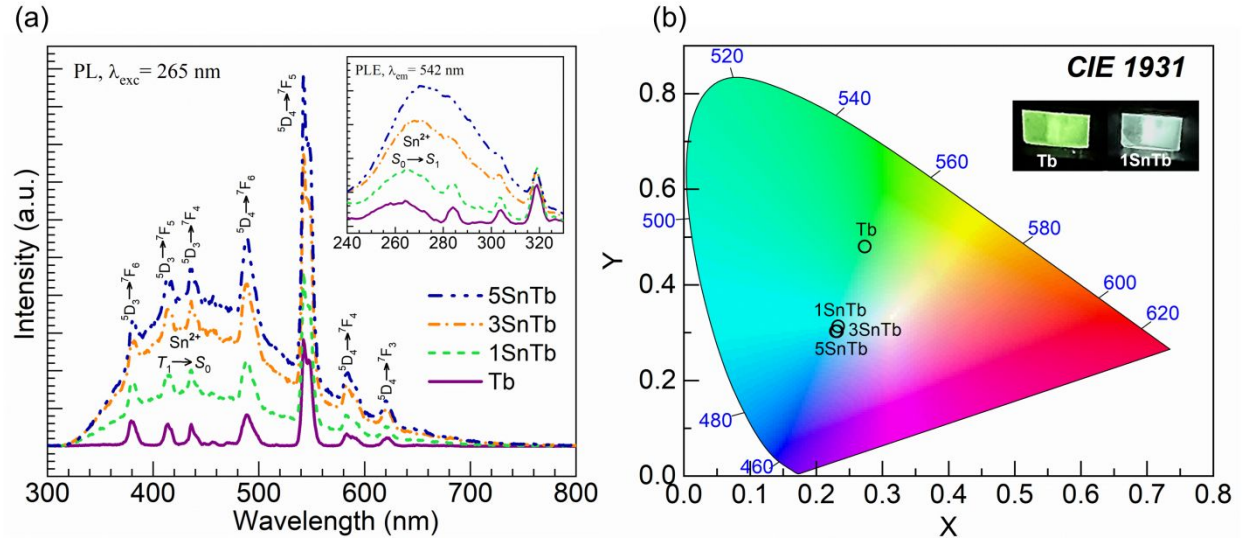

Fig. 9. (a) Emission spectra obtained for the Tb and 1-5SnTb glasses under excitation at 265 nm exhibiting various Tb^{3+} emission lines overlaying the emerging broad emission band attributed to triplet-to-singlet transitions ($T_1 \rightarrow S_0$) in Sn^{2+}. The inset shows the excitation spectra recorded by monitoring emission at 542 nm, showing development of the band attributed to the singlet-to-

singlet excitation ($S_0 \rightarrow S_1$) in Sn^{2+}. (b) The CIE 1931 chromaticity diagram with coordinates of emission color calculated for the glasses from the spectra in panel (a). The inset in panel (b) shows photographs taken in dark for the Tb and 1SnTb glasses under excitation at 265 nm.

Additionally, emission decay curves were obtained for the Tb and 1-5SnTb glasses under excitation at 265 nm by monitoring the emission at 542 nm to assess Tb^{3+} excited state dynamics in connection with the prominent $^5D_4 \rightarrow {}^7F_5$ transition. The recorded traces are shown in Fig. 10. The Tb glass exhibited a signal build-up at first up to about 0.4 ms which is indicative of multi-phonon relaxation processes feeding the $^5D_4$ emitting state from upper energy levels.[46,47] Thereafter, the decay exhibits first-order kinetics. The ms-scale portion following the signal rise was then fit by a single exponential decay function

$$I(t) = I_0 \exp(-t/\tau) \quad (3)$$

where $I(t)$ is the time-dependent luminescence intensity, I_0 the initial intensity, and τ the excited state lifetime. The $^5D_4$ lifetime estimated for the Tb glass was then 2860 (±3) μs. The procedure was applied to the decay curves recorded for the 1SnTb, 3SnTb and 5SnTb glass samples, yielding lifetimes of 2788 (±2), 2803 (±2) and 2847 (±1) μs, respectively (values also displayed in Fig. 10). The deduced lifetimes are overall higher than those reported by Jamalaiah et al.[2] for Tb^{3+}-doped lead telluroborate glasses (within 0.8-0.9 ms). However, they are somewhat lower than those reported by Umamaheswari et al.[3] in sodium fluoro-borate glasses (within 3.0-3.3 ms) and Zhong et al.[15] in SrO–ZnO–P_2O_5 glass (3.3 ms in Tb^{3+} singly-doped). It is noticed herein that the lifetime decreases for the 1SnTb glass relative to the Tb glass. Considering that the tin in the 1SnTb glass occurred mostly as Sn^{4+}, it could be interpreted that an additional decay channel for Tb^{3+} ions is provided by tin(IV). Further on, the 3SnTb and

5SnTb glasses exhibit a trend of lifetime increase for Tb^{3+} ions, however not to the value of the Tb glass. Given that the 3SnTb and 5SnTb contain increasing concentrations of Sn^{2+} estimated at 1.32% and 3.60%, respectively, this may reflect the favorable effect of divalent tin which is acting as energy donor.[4,19,20] Yet, the fact that the lifetimes are still lower than the Tb glass which contains no tin suggests that the presence of Sn^{4+} is detrimental to the PL output. This concurs with the fact that the Tb^{3+} PL intensification as considered above did not follow the Sn^{2+} increments estimated by XANES.

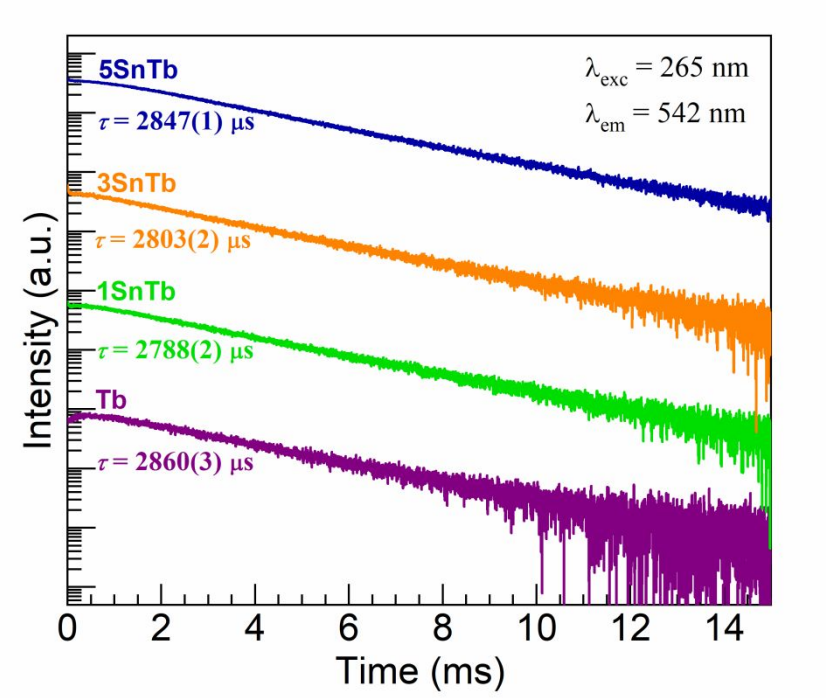

Fig. 10. Emission decay curves obtained for the Tb and 1-5SnTb glasses under excitation at 265 nm by monitoring emission at 542 nm; the deduced Tb^{3+} $^5D_4$ state decay times (τ) are indicated under each trace (uncertainty in last digit shown in parentheses).

4. Conclusions

In brief, barium phosphate glasses were prepared by melting with 0.5 mol% Tb_4O_7 added alongside SnO at 1, 3 and 5 mol%, and the terbium and tin oxidation states were analyzed with the purpose of evaluating their impact on various glass properties. The composition-structure-property study undertaken involved measurements by XRD, Sn K-edge and Tb L_3-edge XANES, Raman spectroscopy, DSC, dilatometry, and PL spectroscopy with decay kinetics assessment. The XRD characterization demonstrated the amorphous nature of the glasses and the lack SnO_2 crystallites, thus supporting the incorporation of tin in the different valence states into the glass structure. While Tb L_3-edge XANES confirmed the occurrence of terbium as Tb^{3+}, the Sn K-edge analysis showed a predisposition for tin to exist as tin(IV), which decreased at high SnO content. The speciation analysis carried out by XANES consequently allowed for evaluating the structural and thermal properties in connection with the impact of tin(IV). The Raman spectroscopy inquiry thus performed agreed with a depolymerization effect substantiated at high tin content but correlating with Sn^{4+} concentration. Likewise, the glass transition and softening temperatures extracted from DSC and dilatometry showed good agreement with the Raman evaluation concerning the predominant effect of tin(IV). Thus, it can be postulated that the higher field strength of Sn^{4+} ions acting as network modifiers increase the Sn–O bond strength underpinning the structural rearrangement in the vicinity of the glass transition. The effect on thermal expansion was however more intricate, as the presence of tin(II) appeared to support a tighter structure. This could be due to the role of divalent tin as network former linking PO_4 tetrahedra. The impact of Sn^{2+} was then evident on the luminescent properties, shifting light emission from the green in merely Tb-doped glass towards the blue-green (cyan) as characterized by the CIE 1931 chromaticity coordinates. The increasing amount of divalent tin in the glasses supported an increase in the overall PL under excitation at 265 nm. The decay

dynamics studied by monitoring Tb^{3+} emission at 542 nm, however, suggested that Sn^{4+} tends to shorten the $^5D_4$ excited state lifetime in Tb^{3+} ions while Sn^{2+} has a favorable effect. Overall, the present work highlights the importance of conducting speciation analysis when investigating material properties rather than just quantifying overall dopant concentration.

Data availability

The data that support the findings of this study are available within the article and from the corresponding author upon reasonable request.

Credit Author Statement

José A. Jiménez: Conceptualization, Visualization, Methodology, Investigation, Formal Analysis, Writing- Original Draft, Reviewing and Editing, Supervision. **Dugan Hayes**: Methodology, Investigation, Formal Analysis, Writing- Original Draft, Reviewing and Editing. **Cali Antolini**: Methodology, Investigation, Formal Analysis. **Benjamin J. Reinhart**: Methodology, Investigation, Formal Analysis.

Conflict of Interest Statement

The authors declare no competing financial interests.

Acknowledgements

This material is based on work supported by the U.S. Department of Energy, Office of Science, Office of Basic Energy Sciences under Award DE-SC0019429, which supported C.A. and D.H.; and the U.S. Department of Energy, Office of Science, Office of Workforce Development for Teachers and Scientists, Office of Science Graduate Student Research

(SCGSR) program, which also supported C.A. The SCGSR program is administered by the Oak Ridge Institute for Science and Education for the DOE under contract number DE-SC0014664. This research used resources of the Advanced Photon Source, a U.S. Department of Energy (DOE) Office of Science User Facility operated for the DOE Office of Science by Argonne National Laboratory under Contract No. DE-AC02-06CH11357. All XANES spectra were collected at beamline 12-BM-B at the Advanced Photon Source, Argonne National Laboratory.

References

[1] J.-L. Yuan, X.-Y. Zeng, J.-T. Zhao, Z.-J. Zhang, H.-H. Chen and X.-X. Yang, *J. Phys. D: Appl. Phys.* 2008, **41**, 105406.

[2] B.C. Jamalaiah, M.V. Vijaya Kumar and K. Rama Gopal, *Physica B*, 2011, **406**, 2871-2875.

[3] D. Umamaheswari, B.C. Jamalaiah, T. Sasikala, T. Chengaiah, Il-Gon Kim and L. Rama Moorthy, *J. Lumin.*, 2012, **132**, 1166-1170.

[4] Z.-m. Wang and G.-y. Gan, *ECS Solid State Letters*, 2014, **3**, R36-R39.

[5] T.-S. Lv, X.-H. Xu, X. Yu and J.-B. Qiu, *J. Am. Ceram. Soc.*, 2015, **98**, 2078-2085.

[6] J. Hu, Y. Zhang, H. Xia, H. Ye, B. Chen and Y. Zhu, *Inorg. Chem.*, 2018, **57**, 7792-7796.

[7] P. Pascuta, L. Pop, R. Stefan, L. Olar, G. Borodi, L.C. Bolundut and E. Culea, *J. Alloys Compd.*, 2019, **799**, 442-449.

[8] A. Gasiorowski and P. Szajerski, *J. Lumin.*, 2019, **214**, 116519.

[9] W. Huang, J. Chen, Y. Li, Y. Wu, L. Li, L. Chen and H. Guo, *Chin. Opt. Lett.*, 2023, **21**, 071601.

[10] Q. Wang and C. Tan, *Anal. Chim. Acta*, 2011, **708**, 111-115.

[11] C. Tan and Q. Wang, *J. Fluoresc.*, 2012, **22**, 1581-1586.

[12] C. Wang, Z. Li and H. Ju, *Anal. Chem.*, 2021, **93**, 14878-14884.

[13] A.K. Singh, *Coord. Chem. Rev.*, 2022, **455**, 214365.

[14] X. Qin, X. Liu, W. Huang, M. Bettinelli and X. Liu, *Chem. Rev.*, 2017, **117**, 4488-4527.

[15] H. Zhong, G. Chen, L. Yao, J. Wang, Y. Yang and R. Zhang, *J. Non-Cryst. Solids*, 2015, **427**, 10-15.

[16] Y.D. Ma, X.S. Peng, M.Z. Fei, W.N. Zhang, L.M. Teng, F.F. Hu, R.F. Wei and H. Guo, *J. Alloys Compd.*, 2020, **846**, 156435.

[17] Q. Ren, Y. Zhao, X. Wu and O. Hai, *Opt. Laser Technol.*, 2021, **136**, 106774.

[18] Y.-P. Qiao, *Mater. Sci. Eng. B*, 2022, **276**, 115565.

[19] H. Masai, Y. Hino, T. Yanagida, Y. Fujimoto and T. Yoko, *Bull. Chem. Soc. Jpn.*, 2014, **87**, 556-563.

[20] A.L Blinov, M.A. Borik, G.E. Malashkevich, I.V. Prusova and A.P. Stupak, *J. Appl. Spectrosc.*, 1998, **63**, 84-87.

[21] J.A. Jiménez, D. Hayes and C. Hasselbrink, *J. Phys. Chem. C*, 2022, **126**, 18421-18428.

[22] J.A. Jiménez and V. Ibarra, *J. Phys. Chem. B*, 2022, **126**, 8579-8587.

[23] J.A. Jiménez, *Phys. Lett. A*, 2023, **462**, 128666.

[24] B. Ravel and M. Newville, *J. Synchrotron Radiat.*, 2005, **12**, 537-541.

[25] XAFS spectrum of Terbium(III,IV) oxide, https://doi.org/10.48505/nims.2490

[26] J. He, C. Yan, M. Huang, R. Shi, Y. Chen, C.D. Ling and Z.-Q. Liu, *Chem. Eur. J.*, 2020, **26**, 5619-5628.

[27] M.A. Smith, M. Chen, Z. Dai, C. Antolini, G.K. Jayasekara, S.K. Yadavalli, B.J. Reinhart, N.P. Padture and D. Hayes, *ACS Appl. Energy Mater.*, 2021, **4**, 4327-4332.

[28] M. Nogami, T. Enomoto and T. Hayakawa, *J. Lumin.*, 2002, **97**, 147-152.

[29] H. Masai, T. Tanimoto, S. Okumura, K. Teramura, S. Matsumoto, T. Yanagida, Y. Tokuda and T. Yoko, *J. Mater. Chem. C*, 2014, **2**, 2137-2143.

[30] J.C. Wang, S. Aswartham, F. Ye, J. Terzic, H. Zheng, D. Haskel, S. Chikara, Y. Choi, P. Schlottmann, R. Custelcean, S.J. Yuan and G. Cao, *Phys. Rev. B*, 2015, **92**, 214411.

[31] D.K. Amarasinghe and F.A. Rabuffetti, *Inorg. Chem.*, 2021, **60**, 3165-3171.

[32] J.E. Pemberton, L. Latifzadeh, J.P. Fletcher and S.H. Risbud, *Chem. Mater.*, 1991, **3**, 195-200.

[33] L. Baia, M. Baia, W. Kiefer, J. Popp and S. Simon, *Chem. Phys.*, 2006, **327**, 63-69.

[34] E. Bekaert, L. Montagne, L. Delevoye, G. Palavit and A. Wattiaux, *J. Non-Cryst. Solids*, 2004, **345-346**, 70-74.

[35] J.A. Jiménez and C. Zhao, Optical absorption, *Mater. Chem. Phys.*, 2014, **147**, 469-475.

[36] J.A. Jiménez, E.R. Fachini and C. Zhao, *J. Mol. Struct.*, 2018, **1164**, 470-474.

[37] J.A. Jiménez and M. Sendova, *J. Phys. Chem. B*, 2023, **127**, 2818-2828.

[38] M. Çelikbilek, A.E. Ersundu, N. Solak and S. Aydin, *J. Alloys Compd.*, 2011, **509**, 5646-5654.

[39] X. He, X. Shen, Q. Huang, J. Zhang, Y. He, T. Liu and A. Lu, *J. Non-Cryst. Solids*, 2021, **559**, 120670.

[40] J. Cha, T. Kubo, H. Takebe and M. Kuwabara, *J. Ceram. Soc. Jpn.*, 2008, **116**, 915-919.

[41] J.W. Lim, S.W. Yung and R.K. Brow, *J. Non-Cryst. Solids*, 2011, **357**, 2690-2694.

[42] H. Segawa, S. Inoue and K. Nomura, *J. Non-Cryst. Solids*, 358, **2012**, 1333-1338.

[43] M.H. Krohn, J.R. Hellmann, B. Mahieu and C.G. Pantano, *J. Non-Cryst. Solids*, 2005, **351**, 455-465.

[44] F. Auzel, in *Radiationless Processes*, edited by B. Di Bartolo, Plenum Press, New York, 1980.

[45] X. Zhang, J. Li, Y.M. Shu, K. Luo, H. Liu, P. Zhang, Y. Huang, G. Liu and Y. Fan, *J. Lumin.*, 2022, **252**, 119305.

[46] G.E. Peterson and P.M. Bridenbaugh, *J. Opt. Soc. Am.*, 1963, **53**, 1129-1138.

[47] C. Armellini, M. Ferrari, M. Montagna, G. Pucker, C. Bernard and A. Monteil, *J. Non-Cryst. Solids*, 1999, **245**, 115-121.